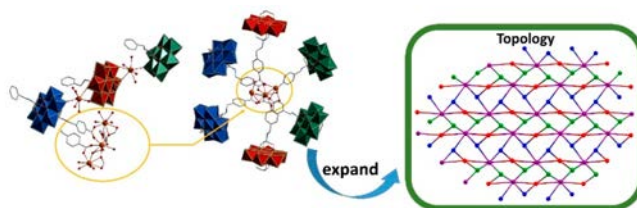


Taking the Third Route for Construction of POMOFs: The First Use of Carboxylate-Functionalized Mn^{III} Anderson–Evans POM-Hybrid Linkers and Lanthanide Nodes

Marcel P. Merkel,* Christopher E. Anson, George E. Kostakis, and Annie K. Powell*

ABSTRACT: The purpose of the present contribution is to illustrate how to design and grow crystals of POMOFs based on POM hybrid linkers with lanthanide ions as nodes. Thus, the Mn^{III} centered Anderson–Evans polyoxometalate (Mn A E POM) was functionalized with 4 (((1,3 dihydroxy 2 (hydroxymethyl) propan 2 yl)amino)methyl)benzoic acid (**H₄L**) to afford the hybrid inorganic–organic POM [N(*n* C₄H₉)₄]₄[(MnMo₆O₁₈)(HL)(L)] (**1**), which in turn reacts with lanthanide salts and yields two three dimensional frameworks with the general formulas Ln(DMF)₆Ln(DMF)₅Ln₃(DMF)₁₀[(MnMo₆O₁₈)(L)₂]₃·*x*DMF (**2**; Ln = La–Nd) and [Ln(DMF)₄(H₂O)]₂[Ln₃(DMF)₆][(MnMo₆O₁₈)(L)₂]₃·*x*DMF (**3**; Ln = Y, Sm–Lu). The differentiation in these two families results from the lanthanide contraction. The crystallization process is crucial for obtaining these two families in a bulk pure phase. Family **2** can be obtained by stirring, while for family **3** the less energy demanding layering method proved to be the most efficient pathway. Notably, the change in the ionic radii causes a change in space group (from *P2₁* (family **2**) to *P2₁/c* (family **3**)); however, the topology of the frameworks is unaffected.



INTRODUCTION

Coordination polymers (CPs), also called metal–organic frameworks (MOFs), are built up using organic building blocks (so called linkers) and inorganic building blocks (so called secondary building units (SBUs)), forming 3D porous frameworks.¹ Here, the linkers contain functional groups, such as carboxylate,^{2,3} amine,⁴ pyridyl,² nitrile,⁵ sulfonate,⁵ and phosphonate,⁶ coordinating to the SBUs, which may be based on Zn,^{3,4} Ni,⁶ Cu,^{2,7} Na,⁵ Ag,⁵ Mg,⁴ Fe,⁸ Cr,⁹ or other metal ions and thus build up a network. Another class of materials are the polyoxometalates (POMs), which are anionic metal oxide clusters composed of transition metals (so called metal addenda atoms; M = W, Mo, Nb, V, Ta) in high oxidation states.^{10,11} A combination of POMs and MOFs results in polyoxometalate based metal–organic frameworks, the so called POMOFs.¹² These compounds may combine and/or improve the properties of POMs and MOFs.^{13–15} This field of research is still in its infancy but is currently receiving an increasing amount of attention due to emergent applications in many fields such as catalysis,^{16–18} proton conduction,^{19,20} sorption,²¹ and electrode materials.¹¹ So far three subgroups of POMOFs have been described in the literature: (1) POMs occupying the cavities of a MOF structure (POM@MOF; Figure 1a),^{17,21–23} (2) POMs used as SBUs in the MOF network (Figure 1b),^{11,24–27} and (3) POMs as part of the linker of the framework (Figure 1c).^{18,28,29} Among all these approaches, the last (route 3) has barely been explored.

So far there do not seem to be any type 3 POMOFs where carboxylate functionalized Anderson–Evans POMs provide hybrid linkers and lanthanide ions act as nodes. This requires the initial synthesis of a suitable organic linker, which in the following step is attached to a polyoxometalate.³⁰ We chose to use the combination of a flexible organic ligand with an Anderson–Evans (A E) POM, as a central part of a linear linker in order to construct a robust framework with lanthanides as nodes. The A E POM has a planar metal {M'M₆} core within the moiety {M'(OH)₆M₆O₂₄}. The simple replacement of M' is hard to achieve; however, starting from the α octamolybdate POM [α Mo₈O₂₆]⁴⁻ provides a relatively easy means to target the desired {M'M₆} through formal replacement of the two tetrahedrally coordinated {MO₄} units above and below the plane with M' in the center of this plane.³¹ In contrast to the postfunctionalization of the hexavanadate hybrid used by Wei et al.,³² we chose 4 (((1,3 dihydroxy 2 (hydroxymethyl)propan 2 yl)amino) methyl)benzoic acid (**H₄L**) as a suitable ligand, with two types of functional groups: the tris(alkoxo) (tris) and the benzoic acid groups. **H₄L** was grafted onto the Mn^{III} centered

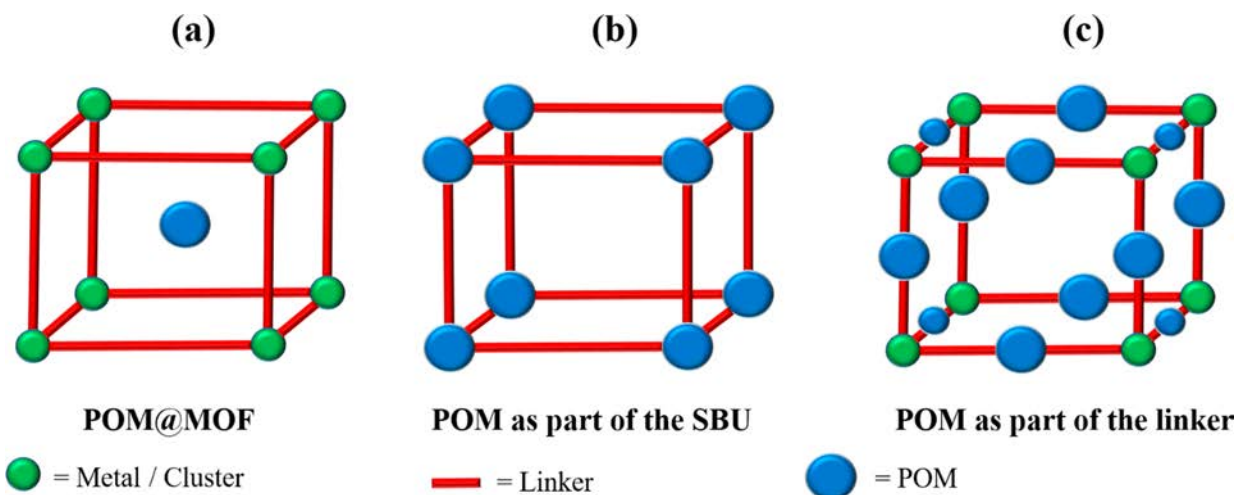


Figure 1. The three subgroups of POMOFs: POMs occupying the cavities of a MOF structure (POM@MOF) (a), POMs used as SBUs in the MOF network (b), and POMs as part of the linker of the framework (c).

Anderson–Evans POM (A E POM) via the hydroxyl groups of the tris group to give $[N(n\text{C}_4\text{H}_9)_4]_4[(\text{MnMo}_6\text{O}_{18})(\text{HL})(\text{L})]$ (**1**). In a next step, the free carboxylate groups and terminal oxygen (O_t) atoms of this hybrid were used in order to coordinate to a series of lanthanides, resulting in two families of frameworks with the general formulas $\text{Ln}(\text{DMF})_6\text{Ln}(\text{DMF})_3\text{Ln}_3(\text{DMF})_{10}[(\text{MnMo}_6\text{O}_{18})(\text{L})_2]_3 \cdot x\text{DMF}$ (**2**; $\text{Ln} = \text{La} - \text{Nd}$) and $[\text{Ln}(\text{DMF})_4(\text{H}_2\text{O})_2][\text{Ln}_3(\text{DMF})_6]_3[(\text{MnMo}_6\text{O}_{18})(\text{L})_2]_3 \cdot x\text{DMF}$ (**3**; $\text{Ln} = \text{Y}, \text{Sm} - \text{Lu}$). In order to simplify complex structures, especially 3D frameworks, a topological analysis can be used to identify and reduce the individual moieties to nodes and connectors in a simplified network. This makes it easier to describe the architecture of the scaffold.^{33–35}

EXPERIMENTAL SECTION

General Considerations. All reagents and solvents were used as received from commercial suppliers without further purification. To determine the carbon, hydrogen, nitrogen, and sulfur fractions of the samples, elemental analysis was carried out using a “Vario Micro Cube” device from PerkinElmer. Infrared spectra were recorded on a PerkinElmer Spectrum GX FT IR spectrometer as KBr pellets in the range $4000 - 400\text{ cm}^{-1}$ with a resolution of 8 cm^{-1} . The following abbreviations are used to describe the peak characteristics: br = broad, sh = shoulder, s = strong, m = medium, and w = weak. NMR spectra of the compounds were measured using Bruker Ultrashield plus 500 (500 MHz) and Varian 500 MHz spectrometers. ^1H and ^{13}C measurements were recorded using deuterated solvents and referenced to tetramethylsilane (TMS) as an internal standard ($\delta = 0\text{ ppm}$). The structures were measured using single crystal X ray diffraction (SCXRD) on area detector diffractometers: IPDS II (Mo $K\alpha$, $\lambda = 0.71073\text{ \AA}$, detector image plate) and STADIVARI (Ga $K\alpha$, $\lambda = 1.34143\text{ \AA}$, detector Dectris Eiger2 R 4 M (detector type HPC)) (STOE). The measurements were taken at temperatures of 150 and 180 K. The crystals were attached to the goniometer head with perfluoroether oil. Powder X ray diffraction (PXRD) measurements were performed on an STOE STADI P diffractometer with Cu $K\alpha$ radiation.

Preparation of 4-HOOC(C₆H₄)CH₂NHC(CH₂OH)₃ (H₄L). Synthesis of the ligand H₄L was performed by an $\text{S}_{\text{N}}2$ reaction between tris(hydroxymethyl)aminomethane and 4 (bromomethyl)benzoic acid. 4 HOOC(C₆H₄)CH₂NHC(CH₂OH)₃ (H₄L) was synthesized according to the literature method.²⁹ 4 (Chloromethyl)benzoic acid (10.0 g, 58.6 mmol) was added over a period of 2 min to a solution of tris(hydroxymethyl)aminomethane (35.6 g, 294 mmol) in 300 mL of

H₂O. The reaction mixture was stirred for 20 h at room temperature, whereas the solid 4 (chloromethyl)benzoic acid was completely dissolved after 30 min and a white precipitate occurred after 7 h of addition. The white precipitate was filtered off and washed with H₂O ($2 \times 20\text{ mL}$) and acetone ($2 \times 15\text{ mL}$), followed by drying under vacuum to yield 10.2 g (68%). The product was characterized using ^1H NMR (DMSO d_6): δ 3.21 (s, 6H), 3.82 (s, 2H), 7.43 (d, 2H), 7.81 (d, 2H).

Preparation of $[N(n\text{-C}_4\text{H}_9)_4]_4[(\text{MnMo}_6\text{O}_{18})(\text{HL})(\text{L})] \cdot 3\text{DMF}$ (1**).** $[N(n\text{C}_4\text{H}_9)_4]_4[\text{Mo}_8\text{O}_{26}]$ was synthesized according to the literature method.³⁶ A mixture of $[N(n\text{C}_4\text{H}_9)_4]_4[\text{Mo}_8\text{O}_{26}]$ (1.100 g, 0.50 mmol), $\text{Mn}(\text{OAc})_3 \cdot 2\text{H}_2\text{O}$ (0.201 g, 0.75 mmol), 4 HOOC(C₆H₄)CH₂NHC(CH₂OH)₃ (H₄L; 0.438 g, 1.71 mmol), tetrabutylammonium bromide (0.215 g, 0.67 mmol), and 20 mL of DMF was stirred for 22 h at 85 °C. The resulting suspension was centrifuged and the orange supernatant was placed in a diethyl ether atmosphere; after 2 days orange crystals had formed. For a higher yield, the diethyl ether diffusion was continued for another 13 days and the crystals were air dried to yield 1.012 g (57% based on Mn; 64% based on Mo). Anal. Calcd for $\text{MnMo}_6\text{O}_{28}\text{C}_{88}\text{N}_6\text{H}_{171}$ (2391.901 g/mol) ($[N(n\text{C}_4\text{H}_9)_4]_4[(\text{MnMo}_6\text{O}_{18})(\text{OCH}_2)_3\text{CNHCH}_2(\text{C}_6\text{H}_4)\text{COOH}][(\text{OCH}_2)_3\text{CNHCH}_2(\text{C}_6\text{H}_4)\text{COO}]]$): C, 44.19; N, 3.51; H, 7.21. Found: C, 44.26; N, 3.58; H, 7.28. FT IR (KBr, cm^{-1}): 3470 (br, m), 2964 (s), 2932 (sh), 2875 (s), 1713 (sh), 1675 (s), 1611 (sh, w), 1479 (s), 1390 (m), 1258 (w), 1156 (w), 1087 (m), 1043 (m), 942 (sh), 922(s), 904 (sh), 771 (sh), 670 (s), 569 (w), 505 (w), 455 (w).

Preparation of $\text{Ln}(\text{DMF})_6\text{Ln}(\text{DMF})_3\text{Ln}_3(\text{DMF})_{10}[(\text{MnMo}_6\text{O}_{18})(\text{L})_2]_3 \cdot x\text{DMF}$ (2**; $\text{Ln} = \text{La} - \text{Nd}$).** A boundary layer of a DMF/MeOH mixture (1/1 v/v, 2 mL) was rapidly pipetted over a solution of $[N(n\text{C}_4\text{H}_9)_4]_4[(\text{MnMo}_6\text{O}_{18})(\text{OCH}_2)_3\text{CNHCH}_2(\text{C}_6\text{H}_4)\text{COOH}][(\text{OCH}_2)_3\text{CNHCH}_2(\text{C}_6\text{H}_4)\text{COO}] \cdot 3\text{DMF}$ (**1**; 10 mg, 0.0042 mmol) dissolved in 1 mL of DMF. A solution of $\text{Ln}(\text{NO}_3)_3 \cdot 5/6\text{H}_2\text{O}$ ($\text{Ln} = \text{La} - \text{Nd}$; 10 mg, 0.0231 mmol) dissolved in 1 mL of MeOH was rapidly pipetted on top to give a three layered system. Yellow crystals of **2** were obtained from the lower layer after 5 days and were dried under vacuum.

The following compounds were synthesized according to the aforementioned layering method.

Compound 2-La Layering. Yield: 4.5 mg (47% based on **1**). Anal. Calcd for $\text{C}_{147}\text{H}_{253}\text{La}_3\text{Mn}_3\text{Mo}_{18}\text{N}_{31}\text{O}_{109}$ (6784.987 g/mol) ($\text{La}(\text{DMF})_6\text{La}(\text{DMF})_3\text{La}_3(\text{DMF})_{10}[(\text{MnMo}_6\text{O}_{18})(\text{OCH}_2)_3\text{CNHCH}_2(\text{C}_6\text{H}_4)\text{COO}]_2 \cdot 4\text{DMF}$): C, 26.02; N, 6.40; H, 3.76. Found: C, 26.15; N, 6.52; H, 3.91. FT IR (KBr, cm^{-1}): 4312 (br, sh), 3315 (br, w), 2930 (m), 2855 (sh), 2817 (sh), 1650 (s), 1612 (sh), 1552 (w), 1499 (w), 1424 (m, sh), 1386 (m), 1303 (w), 1251 (m), 1175 (w), 1115 (m), 1070 (m), 1040 (m), 949 (s), 912 (s), 776 (w), 663 (br, s), 565 (sh), 460 (w), 414 (w).

Compound 2-Ce Layering. Yield: 3.9 mg (42% based on 1). Anal. Calcd for $C_{144}H_{246}N_{30}O_{106}Mn_3Mo_{18}Ce_5$ (6717.945 g/mol) ($Ce(DMF)_6Ce(DMF)_5Ce_3(DMF)_{10}[(MnMo_6O_{18})((OCH_2)_3CNHCH_2(C_6H_4)COO)_2]_3 \cdot 3DMF$): C, 25.75; N, 6.25; H, 3.69. Found: C, 25.64; N, 6.35; H, 3.44. FT IR (KBr, cm^{-1}): 4315 (br, sh), 3317 (br, w), 2932 (m), 2857 (sh), 2820 (sh), 1655 (s), 1613 (sh), 1549 (w), 1501 (w), 1427 (m, sh), 1387 (m), 1300 (w), 1253 (m), 1178 (w), 1118 (m), 1073 (m), 1043 (m), 951 (s), 915 (s), 777 (w), 665 (br, s), 566 (sh), 461 (w), 415 (w).

Compound 2-Pr Layering. Yield: 3.2 mg (35% based on 1). Anal. Calcd for $C_{135}H_{225}N_{27}O_{105}Mn_3Mo_{18}Pr_5$ (6502.622 g/mol) ($Pr(DMF)_6Pr(DMF)_5Pr_3(DMF)_{10}[(MnMo_6O_{18})((OCH_2)_3CNHCH_2(C_6H_4)COO)_2]_3$): C, 24.94; N, 5.82; H, 3.47. Found: C, 25.18; N, 5.44; H, 3.47. FT IR (KBr, cm^{-1}): 4315 (br, sh), 3316 (br, w), 2933 (m), 2858 (sh), 2821 (sh), 1653 (s), 1612 (sh), 1550 (w), 1500 (w), 1428 (m, sh), 1389 (m), 1300 (w), 1251 (m), 1176 (w), 1114 (m), 1071 (m), 1042 (m), 950 (s), 913 (s), 775 (w), 664 (br, s), 563 (sh), 460 (w), 413 (w).

Compound 2-Nd Layering. Yield: 3.7 mg (41% based on 1). Anal. Calcd for $C_{135}H_{225}N_{27}O_{105}Mn_3Mo_{18}Nd_5$ (6519.294 g/mol) ($Nd(DMF)_6Nd(DMF)_5Nd_3(DMF)_{10}[(MnMo_6O_{18})((OCH_2)_3CNHCH_2(C_6H_4)COO)_2]_3$): C, 24.87; N, 5.80; H, 3.48. Found: C, 24.52; N, 5.73; H, 3.46. FT IR (KBr, cm^{-1}): 4310 (br, sh), 3313 (br, w), 2932 (m), 2857 (sh), 2818 (sh), 1651 (s), 1613 (sh), 1553 (w), 1498 (w), 1425 (m, sh), 1387 (m), 1305 (w), 1252 (m), 1176 (w), 1117 (m), 1071 (m), 1041 (m), 948 (s), 913 (s), 777 (w), 664 (br, s), 567 (sh), 461 (w), 415 (w).

In order to obtain larger amounts in a microcrystalline powder form of **2**, $[N(n C_4H_9)_4]_4[(MnMo_6O_{18})((OCH_2)_3CNHCH_2(C_6H_4)COO)((OCH_2)_3CNHCH_2(C_6H_4)COO)] \cdot 3DMF$ (**1**; 200 mg, 0.084 mmol) was dissolved in 20 mL of DMF and a solution of $Ln(NO_3)_3 \cdot 5/6H_2O$ ($Ln = La-Nd$; 200 mg, 0.462 mmol) dissolved in 20 mL of MeOH was added with stirring over a period of 1 min at room temperature. The solution turned turbid within 30 s and was stirred for a further 1.5 h. The resulting powder was dried under vacuum.

The La–Nd containing compounds **2** could best be obtained using a stirring method.

Compound 2-La Stirring. Yield: 76 mg (41% based on 1). Anal. Calcd for $C_{141}H_{239}N_{29}O_{107}Mn_3Mo_{18}La_5$ (6638.799 g/mol) ($La(DMF)_6La(DMF)_5La_3(DMF)_{10}[(MnMo_6O_{18})((OCH_2)_3CNHCH_2(C_6H_4)COO)_2]_3 \cdot 2DMF$): C, 25.51; N, 6.12; H, 3.63. Found: C, 25.33; N, 6.37; H, 3.97. FT IR (KBr, cm^{-1}): 4311 (br, sh), 3317 (br, w), 2931 (m), 2856 (sh), 2815 (sh), 1651 (s), 1613 (sh), 1553 (w), 1498 (w), 1425 (m, sh), 1388 (m), 1304 (w), 1252 (m), 1176 (w), 1116 (m), 1073 (m), 1041 (m), 951 (s), 913 (s), 778 (w), 660 (br, s), 567 (sh), 461 (w), 415 (w).

Compound 2-Ce Stirring. Yield: 77 mg (40% based on 1). Anal. Calcd for $C_{150}H_{260}N_{32}O_{110}Mn_3Mo_{18}Ce_5$ (6864.133 g/mol) ($Ce(DMF)_6Ce(DMF)_5Ce_3(DMF)_{10}[(MnMo_6O_{18})((OCH_2)_3CNHCH_2(C_6H_4)COO)_2]_3 \cdot 5DMF$): C, 26.25; N, 6.53; H, 3.82. Found: C, 26.02; N, 6.74; H, 3.93. FT IR (KBr, cm^{-1}): 4310 (br, sh), 3317 (br, w), 2931 (m), 2856 (sh), 2818 (sh), 1651 (s), 1613 (sh), 1555 (w), 1497 (w), 1423 (m, sh), 1384 (m), 1301 (w), 1254 (m), 1178 (w), 1119 (m), 1073 (m), 1042 (m), 952 (s), 913 (s), 778 (w), 662 (br, s), 567 (sh), 461 (w), 415 (w).

Compound 2-Pr Stirring. Yield: 82 mg (45% based on 1). Anal. Calcd for $C_{135}H_{225}N_{27}O_{105}Mn_3Mo_{18}Pr_5$ (6502.622 g/mol) ($Pr(DMF)_6Pr(DMF)_5Pr_3(DMF)_{10}[(MnMo_6O_{18})((OCH_2)_3CNHCH_2(C_6H_4)COO)_2]_3$): C, 24.94; N, 5.82; H, 3.47. Found: C, 25.13; N, 5.47; H, 3.48. FT IR (KBr, cm^{-1}): 4312 (br, sh), 3315 (br, w), 2931 (m), 2852 (sh), 2817 (sh), 1653 (s), 1612 (sh), 1552 (w), 1489 (w), 1424 (m, sh), 1387 (m), 1305 (w), 1253 (m), 1178 (w), 1117 (m), 1072 (m), 1042 (m), 950 (s), 913 (s), 777 (w), 662 (br, s), 566 (sh), 460 (w), 415 (w).

Compound 2-Nd Stirring. Yield: 79 mg (43% based on 1). Anal. Calcd for $C_{135}H_{225}N_{27}O_{105}Mn_3Mo_{18}Nd_5$ (6519.294 g/mol) ($Nd(DMF)_6Nd(DMF)_5Nd_3(DMF)_{10}[(MnMo_6O_{18})((OCH_2)_3CNHCH_2(C_6H_4)COO)_2]_3$): C, 24.87; N, 5.80; H, 3.48. Found: C, 24.62; N,

5.63; H, 3.56. FT IR (KBr, cm^{-1}): 4312 (br, sh), 3315 (br, w), 2932 (m), 2855 (sh), 2819 (sh), 1650 (s), 1613 (sh), 1552 (w), 1497 (w), 1424 (m, sh), 1386 (m), 1306 (w), 1251 (m), 1175 (w), 1116 (m), 1070 (m), 1042 (m), 949 (s), 914 (s), 776 (w), 663 (br, s), 566 (sh), 460 (w), 414 (w).

Preparation of $[Ln(DMF)_4(H_2O)_2][Ln_3(DMF)_6][(MnMo_6O_{18})((OCH_2)_3CNHCH_2(C_6H_4)COO)_2]_3 \cdot xDMF$ (3**; $Ln = Y, Sm-Lu$).** A boundary layer of a DMF/MeOH mixture (1/1 v/v, 2 mL) was rapidly pipetted over a solution of $[N(n C_4H_9)_4]_4[(MnMo_6O_{18})((OCH_2)_3CNHCH_2(C_6H_4)COO)((OCH_2)_3CNHCH_2(C_6H_4)COO)] \cdot 3DMF$ (**1**; 10 mg, 0.0042 mmol) dissolved in 1 mL of DMF. A solution of $Ln(NO_3)_3 \cdot 5/6H_2O$ ($Ln = Y, Sm-Lu$; 10 mg, 0.0231 mmol) dissolved in 1 mL of MeOH was rapidly pipetted on top to give a three layered system. Yellow crystals of **3** were obtained from the lower layer after 5 days and were dried under vacuum.

The following compounds were synthesized according to the aforementioned layering method.

Compound 3-Y Layering. Yield: 3.2 mg (35% based on 1). Anal. Calcd for $C_{138}H_{236}N_{28}O_{108}Mn_3Y_3Mo_{18}$ (6351.738 g/mol) ($[Y(DMF)_4(H_2O)_2][Y_3(DMF)_6][(MnMo_6O_{18})((OCH_2)_3CNHCH_2(C_6H_4)COO)_2]_3 \cdot 8DMF$): C, 26.09; N, 6.18; H, 3.75. Found: C, 25.76; N, 6.44; H, 4.11. FT IR (KBr, cm^{-1}): 4314 (br, sh), 3315 (br, w), 2930 (m), 2855 (sh), 2817 (sh), 1650 (s), 1613 (sh), 1552 (w), 1450 (w), 1424 (m, sh), 1386 (m), 1304 (w), 1251 (m), 1175 (w), 1165 (m), 1070 (m), 1040 (m), 952 (s), 912 (s), 776 (w), 665 (br, s), 565 (sh), 460 (w), 412 (w).

Compound 3-Sm Layering. Yield: 4.5 mg (52% based on 1). Anal. Calcd for $C_{120}H_{194}N_{22}O_{102}Mn_3Sm_3Mo_{18}$ (6220.446 g/mol) ($[Sm(DMF)_4(H_2O)_2][Sm_3(DMF)_6][(MnMo_6O_{18})((OCH_2)_3CNHCH_2(C_6H_4)COO)_2]_3 \cdot 2DMF$): C, 23.17; N, 4.95; H, 3.14. Found: C, 23.01; N, 5.20; H, 3.45. FT IR (KBr, cm^{-1}): 4313 (br, sh), 3313 (br, w), 2930 (m), 2855 (sh), 2819 (sh), 1650 (s), 1613 (sh), 1554 (w), 1499 (w), 1425 (m, sh), 1386 (m), 1305 (w), 1251 (m), 1177 (w), 1117 (m), 1071 (m), 1041 (m), 949 (s), 912 (s), 776 (w), 665 (br, s), 565 (sh), 462 (w), 414 (w).

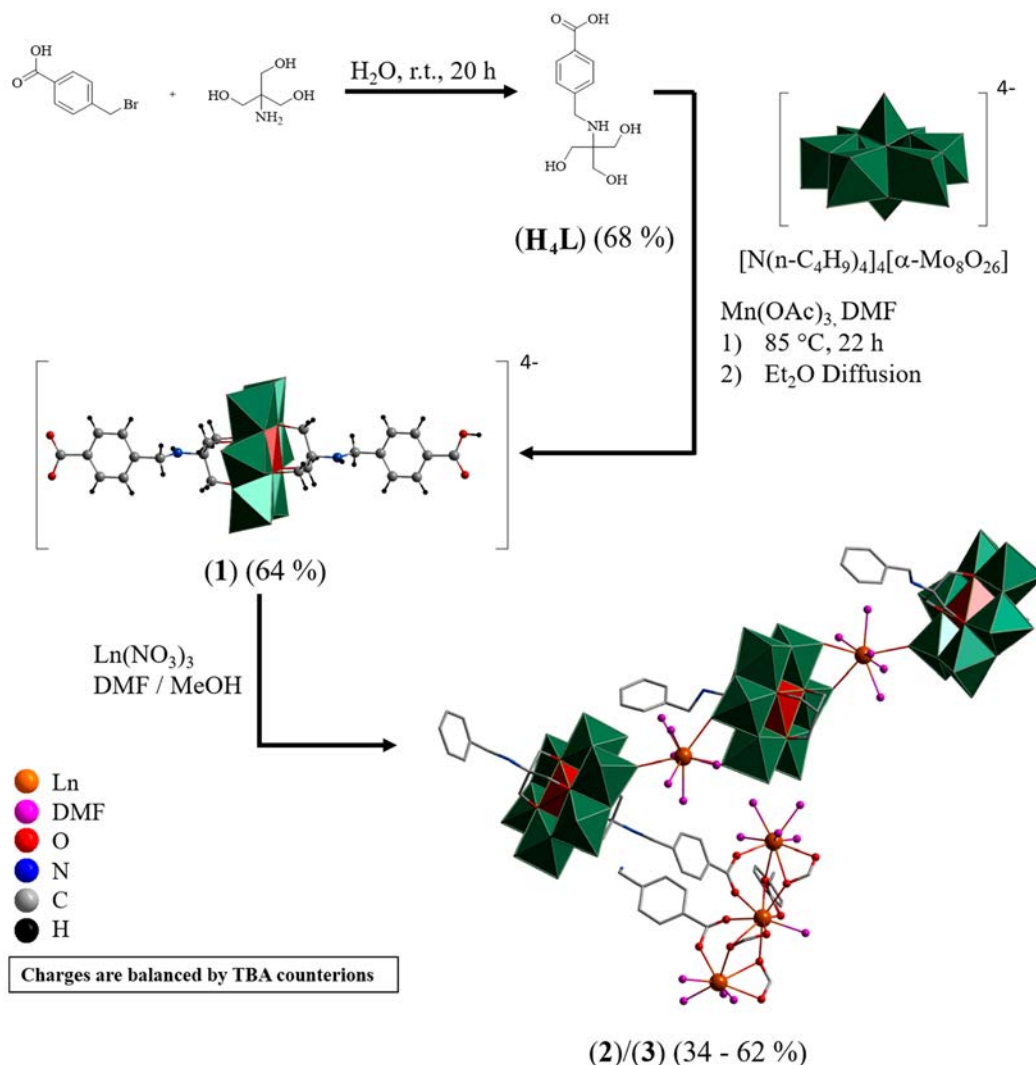
Compound 3-Eu Layering. Yield: 5.6 mg (62% based on 1). Anal. Calcd for $C_{129}H_{215}N_{25}O_{105}Mn_3Mo_{18}Eu_3$ (6447.747 g/mol) ($[Eu(DMF)_4(H_2O)_2][Eu_3(DMF)_6][(MnMo_6O_{18})((OCH_2)_3CNHCH_2(C_6H_4)COO)_2]_3 \cdot 5DMF$): C, 24.03; N, 5.43; H, 3.36. Found: C, 23.95; N, 5.71; H, 3.60. FT IR (KBr, cm^{-1}): 4313 (br, sh), 3315 (br, w), 2930 (m), 2856 (sh), 2817 (sh), 1650 (s), 1612 (sh), 1553 (w), 1499 (w), 1424 (m, sh), 1386 (m), 1305 (w), 1251 (m), 1175 (w), 1114 (m), 1070 (m), 1042 (m), 949 (s), 912 (s), 778 (w), 665 (br, s), 565 (sh), 460 (w), 414 (w).

Compound 3-Gd Layering. Yield: 3.6 mg (42% based on 1). Anal. Calcd for $C_{117}H_{187}N_{21}O_{101}Mn_3Mo_{18}Gd_3$ (6181.802 g/mol) ($[Gd(DMF)_4(H_2O)_2][Gd_3(DMF)_6][(MnMo_6O_{18})((OCH_2)_3CNHCH_2(C_6H_4)COO)_2]_3 \cdot DMF$): C, 22.73; N, 4.76; H, 3.05. Found: C, 22.37; N, 4.95; H, 3.35. FT IR (KBr, cm^{-1}): 4312 (br, sh), 3317 (br, w), 2930 (m), 2855 (sh), 2819 (sh), 1650 (s), 1613 (sh), 1552 (w), 1499 (w), 1424 (m, sh), 1388 (m), 1303 (w), 1251 (m), 1175 (w), 1118 (m), 1070 (m), 1040 (m), 949 (s), 913 (s), 776 (w), 663 (br, s), 565 (sh), 462 (w), 414 (w).

Compound 3-Tb Layering. Yield: 4.1 mg (45% based on 1). Anal. Calcd for $C_{129}H_{215}N_{25}O_{105}Mn_3Mo_{18}Tb_3$ (6482.554 g/mol) ($[Tb(DMF)_4(H_2O)_2][Tb_3(DMF)_6][(MnMo_6O_{18})((OCH_2)_3CNHCH_2(C_6H_4)COO)_2]_3 \cdot 5DMF$): C, 23.90; N, 5.40; H, 3.42. Found: C, 23.75; N, 5.56; H, 3.58. FT IR (KBr, cm^{-1}): 4312 (br, sh), 3315 (br, w), 2930 (m), 2855 (sh), 2818 (sh), 1650 (s), 1612 (sh), 1556 (w), 1498 (w), 1424 (m, sh), 1387 (m), 1303 (w), 1251 (m), 1176 (w), 1115 (m), 1071 (m), 1040 (m), 948 (s), 912 (s), 776 (w), 663 (br, s), 566 (sh), 460 (w), 415 (w).

Compound 3-Dy Layering. Yield: 4.2 mg (48% based on 1). Anal. Calcd for $C_{117}H_{187}Dy_3Mn_3Mo_{18}N_{21}O_{101}$ (6208.411 g/mol) ($[Dy(DMF)_4(H_2O)_2][Dy_3(DMF)_6][(MnMo_6O_{18})((OCH_2)_3CNHCH_2(C_6H_4)COO)_2]_3 \cdot DMF$): C, 22.63; N, 4.74; H, 3.04. Found: C, 22.51; N, 5.06; H, 3.38. FT IR (KBr, cm^{-1}): 4312 (br, sh), 3315 (br, w), 2931 (m), 2855 (sh), 2817 (sh), 1651 (s), 1612 (sh), 1552 (w), 1499 (w), 1425 (m, sh), 1386 (m), 1304 (w), 1251 (m), 1175 (w), 1115

Scheme 1. Synthetic Path of This Work: Starting from the Synthesis of the Organic Ligand LH₄, Followed by Its Use to Form 1 (L–POM–L), Which Was Then Further Reacted with Ln(NO₃)₃ in Order to Form Families 2 and 3



(m), 1071 (m), 1040 (m), 949 (s), 912 (s), 775 (w), 663 (br, s), 565 (sh), 461 (w), 414 (w).

Compound 3-Ho Layering. Yield: 4.0 mg (43% based on 1). Anal. Calcd for C₁₂₆H₂₀₈N₂₄O₁₀₄Mn₃Mo₁₈Ho₅ (6439.485 g/mol) ([Ho(DMF)₄(H₂O)]₂[Ho₃(DMF)₆][[(MnMo₆O₁₈)((OCH₂)₃CNHCH₂(C₆H₄)COO)₂]₃·4DMF): C, 23.50; N, 5.22; H, 3.26. Found: C, 23.26; N, 5.44; H, 3.58. FT IR (KBr, cm⁻¹): 4312 (br, sh), 3316 (br, w), 2930 (m), 2855 (sh), 2817 (sh), 1651 (s), 1612 (sh), 1552 (w), 1499 (w), 1426 (m, sh), 1386 (m), 1305 (w), 1251 (m), 1175 (w), 1116 (m), 1070 (m), 1041 (m), 949 (s), 912 (s), 776 (w), 665 (br, s), 565 (sh), 461 (w), 414 (w).

Compound 3-Er Layering. Yield: 3.8 mg (39% based on 1). Anal. Calcd for C₁₄₇H₂₅₇N₃₁O₁₁₁Mn₃Mo₁₈Er₅ (6962.785 g/mol) ([Er(DMF)₄(H₂O)]₂[Er₃(DMF)₆][[(MnMo₆O₁₈)((OCH₂)₃CNHCH₂(C₆H₄)COO)₂]₃·11DMF): C, 25.36; N, 6.24; H, 3.72. Found: C, 24.98; N, 6.45; H, 3.93. FT IR (KBr, cm⁻¹): 4312 (br, sh), 3316 (br, w), 2930 (m), 2856 (sh), 2817 (sh), 1650 (s), 1613 (sh), 1552 (w), 1499 (w), 14254 (m, sh), 1386 (m), 1305 (w), 1251 (m), 1175 (w), 1115 (m), 1071 (m), 1040 (m), 949 (s), 913 (s), 776 (w), 663 (br, s), 566 (sh), 460 (w), 414 (w).

Compound 3-Tm Layering. Yield: 3.4 mg (35% based on 1). Anal. Calcd for C₁₄₇H₂₅₇N₃₁O₁₁₁Mn₃Mo₁₈Tm₅ (6971.161 g/mol) ([Tm(DMF)₄(H₂O)]₂[Tm₃(DMF)₆][[(MnMo₆O₁₈)((OCH₂)₃CNHCH₂(C₆H₄)COO)₂]₃·11DMF): C, 25.33; N, 6.23; H, 3.72. Found: C, 25.22; N, 6.46; H, 3.89. FT IR (KBr, cm⁻¹): 4313 (br, sh), 3315 (br,

w), 2931 (m), 2855 (sh), 2817 (sh), 1651 (s), 1612 (sh), 1552 (w), 1499 (w), 1422 (m, sh), 1386 (m), 1303 (w), 1252 (m), 1175 (w), 1115 (m), 1071 (m), 1040 (m), 949 (s), 912 (s), 778 (w), 663 (br, s), 565 (sh), 461 (w), 414 (w).

Compound 3-Yb Layering. Yield: 3.8 mg (44% based on 1). Anal. Calcd for C₁₂₉H₂₁₅N₂₅O₁₀₅Mn₃Mo₁₈Yb₅ (6553.127 g/mol) ([Yb(DMF)₄(H₂O)]₂[Yb₃(DMF)₆][[(MnMo₆O₁₈)((OCH₂)₃CNHCH₂(C₆H₄)COO)₂]₃·SDMF): C, 23.64; N, 5.34; H, 3.31. Found: C, 23.93; N, 5.71; H, 3.38. FT IR (KBr, cm⁻¹): 4312 (br, sh), 3315 (br, w), 2932 (m), 2855 (sh), 2817 (sh), 1652 (s), 1612 (sh), 1552 (w), 1499 (w), 1426 (m, sh), 1386 (m), 1303 (w), 1253 (m), 1175 (w), 1117 (m), 1070 (m), 1041 (m), 949 (s), 912 (s), 775 (w), 663 (br, s), 566 (sh), 460 (w), 415 (w).

Compound 3-Lu Layering. Yield: 3.1 mg (34% based on 1). Anal. Calcd for C₁₂₉H₂₁₅N₂₅O₁₀₅Mn₃Mo₁₈Lu₅ (6562.762 g/mol) ([Lu(DMF)₄(H₂O)]₂[Lu₃(DMF)₆][[(MnMo₆O₁₈)((OCH₂)₃CNHCH₂(C₆H₄)COO)₂]₃·SDMF): C, 23.61; N, 5.34; H, 3.30. Found: C, 23.24; N, 5.66; H, 3.65. FT IR (KBr, cm⁻¹): 4313 (br, sh), 3315 (br, w), 2932 (m), 2855 (sh), 2817 (sh), 1651 (s), 1612 (sh), 1553 (w), 1499 (w), 1425 (m, sh), 1386 (m), 1305 (w), 1251 (m), 1175 (w), 1116 (m), 1070 (m), 1040 (m), 949 (s), 913 (s), 776 (w), 663 (br, s), 565 (sh), 461 (w), 414 (w).

In order to obtain larger amounts of a microcrystalline powder form of Dy containing 3, [N(n-C₄H₉)₄]₄[(MnMo₆O₁₈)((OCH₂)₃

CNHCH₂(C₆H₄)COOH)((OCH₂)₃CNH(C₆H₄)COO)]₃·3DMF (**1**; 200 mg, 0.084 mmol) was dissolved in 20 mL of DMF and a solution of Dy(NO₃)₃·6H₂O (200 mg, 0.462 mmol) dissolved in 20 mL of MeOH was added with stirring over a period of 1 min at room temperature. The solution turned turbid within 30 s and was stirred for a further 1.5 h. The resulting powder was dried under vacuum to yield 78 mg (40% based on **1**). Anal. Calcd for C₁₅₀H₂₆₄Dy₃Mn₃Mo₁₈N₃₂O₁₁₂ (7012.443 g/mol) ([Dy(DMF)₄(H₂O)]₂[Dy₃(DMF)₆][[(MnMo₆O₁₈)((OCH₂)₃CNHCH₂(C₆H₄)COO)]₃·12DMF): C, 25.69; N, 6.39; H, 3.79. Found: C, 25.42; N, 6.12; H, 3.96. FT IR (KBr, cm⁻¹): 4313 (br, sh), 3315 (br, w), 2931 (m), 2855 (sh), 2817 (sh), 1651 (s), 1613 (sh), 1552 (w), 1499 (w), 1425 (m, sh), 1386 (m), 1305 (w), 1251 (m), 1176 (w), 1115 (m), 1071 (m), 1040 (m), 949 (s), 913 (s), 776 (w), 663 (br, s), 566 (sh), 460 (w), 415 (w).

RESULTS AND DISCUSSION

Scheme 1 shows the synthetic path of this work. The ligand H₄L was synthesized using the S_N2 reaction between 4 (chloromethyl)benzoic acid and tris(hydroxymethyl)aminomethane at room temperature in water.³⁷ This organic ligand H₄L was then reacted with [N(n C₄H₉)₄][α Mo₈O₂₆],³⁶ Mn^{III}(OAc)₃·2H₂O, and tetrabutylammonium bromide (TBA Br) in DMF at 85 °C, forming compound **1** (L–POM–L). The two tetrahedrally coordinated Mo^{VI} ions above and below the planar ring structure of the [α Mo₈O₂₆]⁴⁻ moiety are now absent and the Mn^{III} ion originating from Mn(OAc)₃ is inserted in the center of the ring. Additionally, two triply deprotonated organic ligands HL³⁻ are grafted onto the resulting A E POM. This POM hybrid was then combined with lanthanide ions from Ln(NO₃)₃ to form type 3 POMOFs, where the POM is present as part of the linker and the nodes are the lanthanide ions.

The structure of **1** is shown in Figure 2a, and the crystallographic data are given in Table S1. The core of this

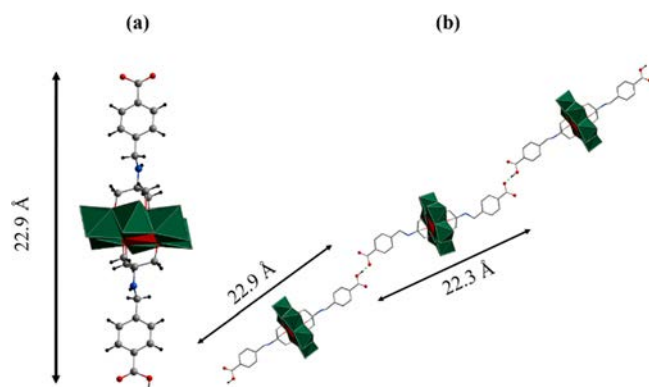


Figure 2. L–POM–L hybrid in **1**: single hybrid (a) and 1D “zigzag” chains (b). Color code: A E POM, green ring with red polyhedral models; O, red; C, gray; N, blue; H, black. TBA counterions and DMF molecules are omitted for clarity. For (b), the C and N atoms are shown with a wire/stick design and only H atoms of carboxylate groups are shown.

compound is the Mn A E POM {Mn^{III}Mo^{VI}₆O₁₈} with the ligand L³⁻ attached to it via the deprotonated hydroxyl groups, above and below the plane. Additionally, one of the carboxylate groups of each hybrid is deprotonated, resulting in a total charge of 4–, which is balanced by four TBA counterions. The six Mo^{VI} metal addenda atoms and the central heteroatom Mn^{III} have an octahedral coordination geometry, and the coordination sites of Mn^{III} are completed by

six oxo ligands, which are further shared with the organic ligand and Mo^{VI} centers of the surrounding octahedra. The length of the L–POM–L hybrid linker is either 22.3 or 22.9 Å. In addition, there are three DMF molecules per asymmetric unit in the lattice; one of these was identified via the SQUEEZE function within PLATON.³⁸

In the crystal structure of **1** the individual [(MnMo₆O₁₈)(HL)(L)]⁴⁻ hybrids form zigzag chains via hydrogen bonds between two carboxylate groups of the organic ligands of two different hybrid units with an O···O distance of 2.420(5) Å and an O–H···O angle of 163.6° (Figure 2b).

Figure 3 shows an extract of the chains formed by the POM hybrids in views along the *a*, *b*, and *c* axes. In the structure, two types of L–POM–L units form the chains resulting in two types of chains with an A–B alternation.

For a better understanding, these two types of links within the chains are colored in red and green. The view along the *b* axis (Figure 3b) reveals that each chain is formed by an A–B alternation of green and red hybrids. It also shows that, in the *a*–*c* plane, the chains lie parallel to each other. The shortest distance between two terminal oxygen atoms of two neighboring polyanions is 8.7 Å. In the *b*–*c* plane (Figure 3a) and the *a*–*b* plane (Figure 3c) the chains have tilt angles of 107.5 and 96.3°, respectively.

Figure 4 shows the simulated (simu) and experimental (exp) PXRD patterns of **1**. The 2θ values of the reflections of **1** exp shows a good agreement with those of **1** simu.

The reaction of the hybrid compound **1** with lanthanide metals (Ln = Y, La–Lu) results in two families of frameworks with the formulas Ln(DMF)₆Ln(DMF)₅Ln₃(DMF)₁₀ [(MnMo₆O₁₈)((OCH₂)₃CNHCH₂(C₆H₄)COO)]₃·xDMF (**2**; Ln = La–Nd) and [Ln(DMF)₄(H₂O)]₂[Ln₃(DMF)₆][(MnMo₆O₁₈)((OCH₂)₃CNHCH₂(C₆H₄)COO)]₃·xDMF (**3**; Ln = Y, Sm–Lu). The differentiation in these two families results from the lanthanide contraction, where the later lanthanide ions have significantly smaller ionic radii in comparison to the earlier ions. This also explains the decrease in coordination sites at the lanthanide centers with increasing atomic number within the lanthanide series. Two approaches to obtaining single crystals were explored: namely, a layering and a stirring method. In the case of the layering method, a boundary layer of a mixture of DMF/MeOH (1/1 v/v) was rapidly pipetted over a solution of **1** dissolved in DMF in order to avoid mixing of the solvents. Then a solution of Ln(NO₃)₃·5/6H₂O (Ln = Y, La–Lu) dissolved in MeOH was rapidly pipetted on top to give a three layered system. Yellow crystals of the families of **2** and **3**, respectively, were obtained from the lower layer after 5 days and were dried under vacuum (yield: 34–62%). In the case of the stirring method, **1** was dissolved in DMF and a solution of Ln(NO₃)₃·5/6H₂O (Ln = Y, La–Lu) dissolved in MeOH was added with stirring over a period of 1 min at room temperature. The solution turned turbid within 30 s and was stirred for a further 1.5 h. The resulting powder was dried under vacuum (yield: 40–45% based on **1** depending on Ln = Y, La–Lu). For the description of the family **2**, the Ce³⁺ compound is chosen as representative for the other structures. The crystallographic data of this compound are given in Table S2. As shown in Figure 5, the structure of **2** consists of three {(MnMo₆O₁₈)((OCH₂)₃CNHCH₂(C₆H₄)COO)]₃⁵⁻ units plus one {Ce(DMF)₆}³⁺, one {Ce(DMF)₅}³⁺, and one {Ce₃(DMF)₁₀}⁹⁺ unit.

To simplify the description of the structure, A E POMs with different connection modes are marked in different colors in

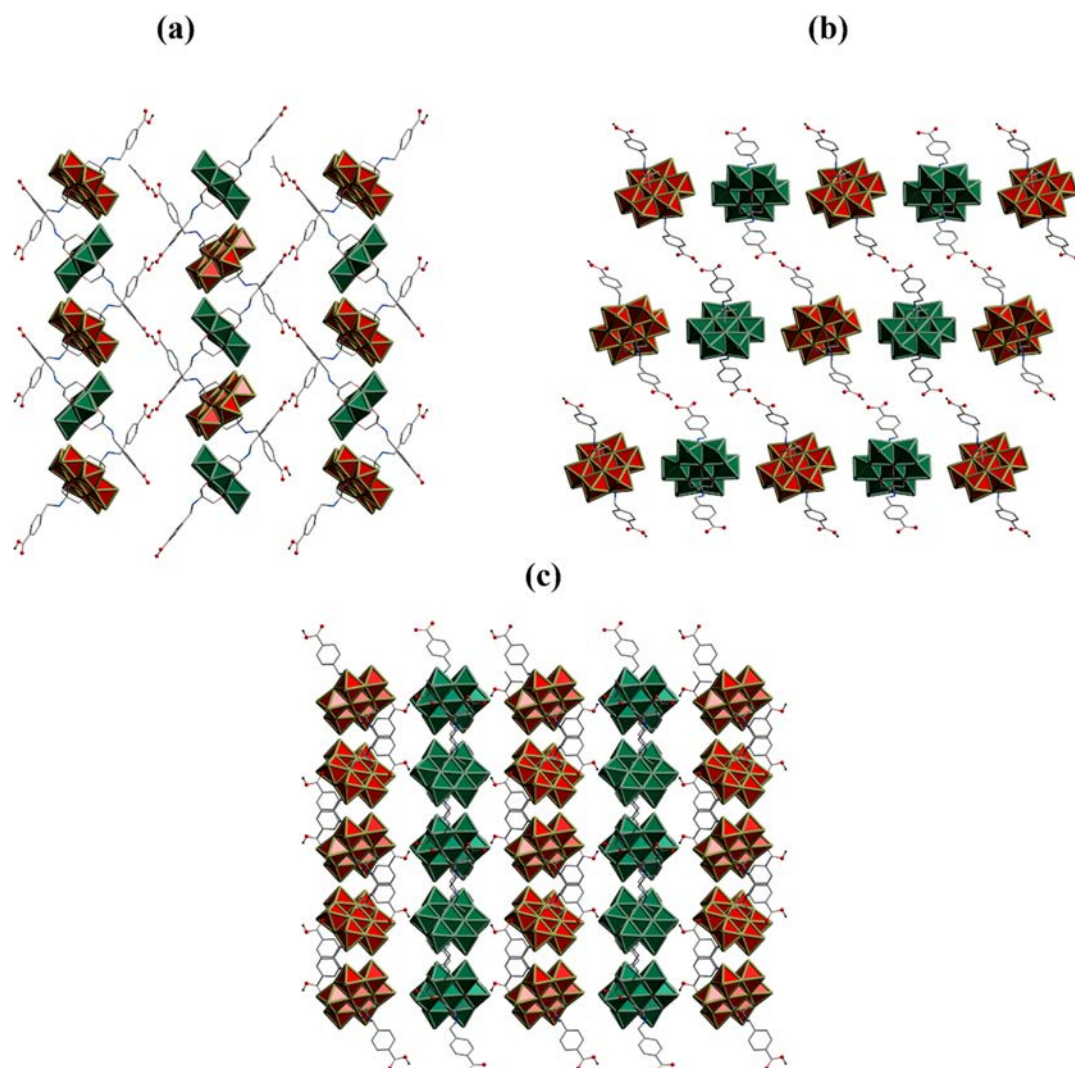


Figure 3. Views along the *a* axis (a), *b* axis, (b) and *c* axis (c) of the crystal structure of **1**. Color code: A E POMs, green and red polyhedral models; O, red, H (only of carboxylate groups), black; C, gray wire/stick; N, blue wire stick. TBA counterions and DMF molecules are omitted for clarity.

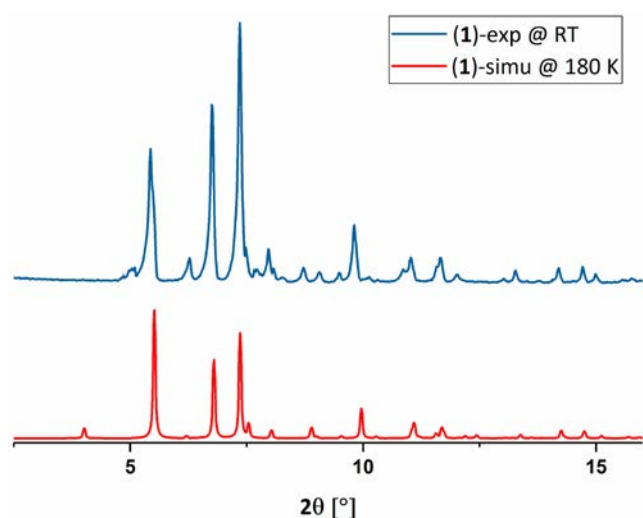


Figure 4. Simulated (simu) and experimental (exp) PXRD patterns of **1**.

Figure 6. Figure 6a reveals that the A E POM hybrid shown in green links to the $\{\text{Ce}(\text{DMF})_5\}^{3+}$ unit with Ce2 (unit 2) as the central atom via one terminal oxygen (O_t) atom. Another A E POM hybrid colored in red also binds to this Ce2 (unit 2) atom via two O_t atoms opposite to the green A E POM. This red A E POM hybrid is then attached to one $\{\text{Ce}(\text{DMF})_6\}^{3+}$ moiety with Ce1 (unit 1) as its center through two O_t atoms, which lie opposite to the two O_t atoms coordinating to the first $\{\text{Ce}(\text{DMF})_5\}^{3+}$ unit. A third A E POM hybrid shown in blue binds to the $\{\text{Ce}(\text{DMF})_6\}^{3+}$ unit via one O_t atom opposite to those of the red A E POM. This blue A E POM hybrid also links via a carboxylate group, which is part of the organic linker, to a $\{\text{Ce}_3(\text{DMF})_{10}\}^{9+}$ unit containing Ce3, Ce4, and Ce5 (unit 3). As shown in Figure 6b) five additional A E POMs coordinate to this $\{\text{Ce}_3(\text{DMF})_{10}\}^{9+}$ unit via carboxylate groups coming from two green, two blue, and two red A E POM hybrids. The $\{\text{Ce}_3(\text{DMF})_{10}\}^{9+}$ moiety is hexagonally coordinated by the six A E POMs.

The distance between the Ce^{3+} centers in the $\{\text{Ce}(\text{DMF})_5\}^{3+}$ (unit 2) and the $\{\text{Ce}(\text{DMF})_6\}^{3+}$ (unit 1) units is 12.4 Å, whereas the distances between two Mn atoms of the POM moieties are about 12.2 Å. The Mn–Ce distances

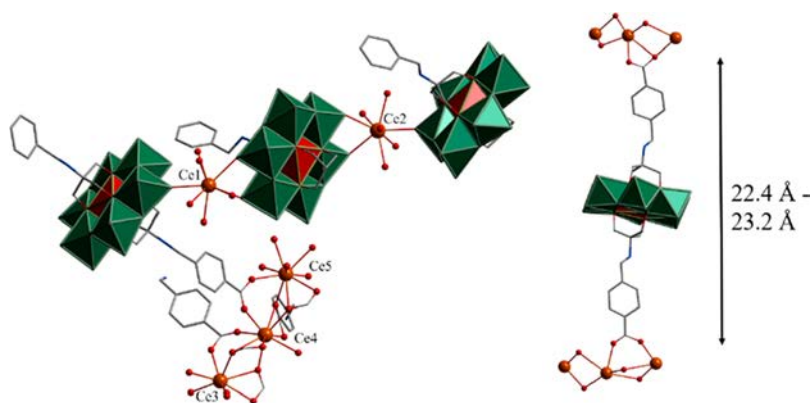


Figure 5. Structure of **2 Ce**. Color code: A E POMs, green ring with red polyhedral models; Ce, orange; O, red; C, gray wire/stick; N, blue wire/stick. Lattice DMF molecules and H atoms are omitted for clarity. DMF molecules coordinating to Ce atoms are represented by their O atoms.

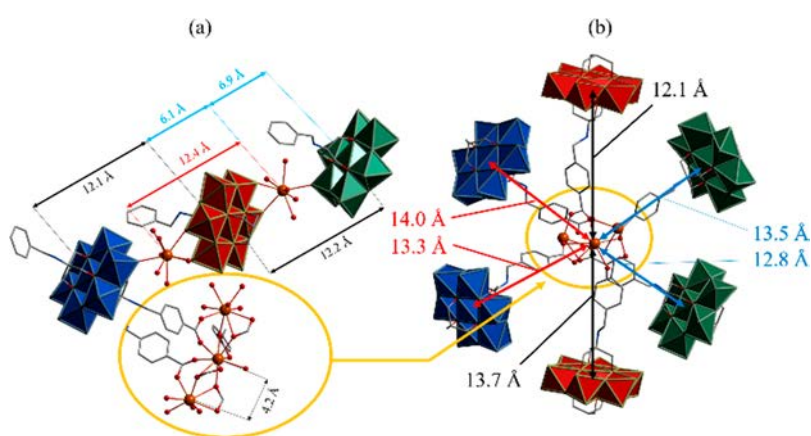


Figure 6. (a) Structure of **2 Ce**. DMF molecules and H atoms are omitted for clarity. (b) Six A E POMs coordinating to $\{\text{Ce}_3(\text{DMF})_{10}\}^{9+}$ unit via carboxylate groups. Color code: A E POMs, green, red, blue polyhedral models; Ce, orange; O, red; C, gray wire/stick; N, blue wire/stick. Lattice DMF molecules and H atoms are omitted for clarity. DMF molecules coordinating to Ce atoms are represented by their O atoms.

between a core of a hybrid and a Ce ion of the $\{\text{Ce}(\text{DMF})_5\}^{3+}$ (unit 2) and the $\{\text{Ce}(\text{DMF})_6\}^{3+}$ (unit 1) parts, respectively, are 6.1 and 6.9 Å. The Ce–Ce distances within the $\{\text{Ce}_3(\text{DMF})_{10}\}^{9+}$ (unit 3) unit are 4.2 Å, whereas the Ce–Mn distance between the Ce_3 unit and a hybrid ranges from 12.1 to 14.0 Å. The largest $\text{O}_{\text{COO}}-\text{O}_{\text{COO}}$ distances within one POM hybrid range from 22.4 to 23.2 Å. In comparison to the hybrid linker compound **1**, the hybrids in **2 Ce** are on average compressed by 0.3 Å. In **2 Ce** several DMF molecules, which coordinate to the Ce centers, are disordered. For this reason, only the O atoms of two DMF molecules of the $\{\text{Ce}(\text{DMF})_6\}^{3+}$ (unit 2) unit, one DMF molecule of the $\{\text{Ce}(\text{DMF})_5\}^{3+}$ (unit 1) moiety, and six DMF molecules of the $\{\text{Ce}_3(\text{DMF})_{10}\}^{9+}$ (unit 3) part could be refined. Furthermore, only 2 DMF molecules in the lattice could be crystallographically identified, whereas 15 additional DMF molecules are suggested via the SQUEEZE function within PLATON.³⁸ The green A E POM is disordered. During the refinement process, it was not possible to model this disorder with partial occupancy atoms, only as single components with highly anisotropic thermal ellipsoids with significant residual electron density surrounding this polyanion. When the A E POM is considered to be wheel, the organic parts $\{(\text{OCH}_2)_3\text{CNHCH}_2(\text{C}_6\text{H}_4)\text{COO}\}$ correspond to its axle. The POM can rotate around this axis and is bonded to just one Ce2 atom, so that the POM can undergo a high amplitude of vibration. The amplitude of the vibration of the atoms

within the POM increases as we move farther from the central Mn atom. Due to the fact that the organic ligands are not linear, with the C–N bond forming a kink, this organic part is also 2 fold disordered about the direction of rotation. For some of these ligands this disorder could be modeled, but for others it was necessary to use one set of highly anisotropic atoms.

The SHAPE³⁹ analysis shows that the Ce^{3+} ions are square antiprismatic (SAPR) (eight coordinated Ce2 and Ce3) and capped square antiprismatic (CSAPR) (nine coordinated Ce1, Ce4, Ce5) coordinated (Table S4 and Figure S23).

Figure 7 shows the PXRD patterns of the family **2 Ln** with $\text{Ln} = \text{La}-\text{Nd}$. The simulated pattern (**2 Ce simu**) serves as a reference. From all of the PXRD patterns of **2 Ln**, it is clearly seen that the samples contain the desired products. However, the patterns with the labeling “L” (synthesized via a layering method) show some extra reflections at e.g. 2θ values of 6.2, 8.8, 10.8, and 24.1° , respectively. This reveals that during the crystallization process at least one other unknown compound crystallizes. It was found that the formation of this byproduct could be avoided by using a stirring method (labeled in Figure 7 with “S”).

For q description of the structure of the 3 series, Dy was chosen as a representative for Ln. The crystallographic data of this compound are given in Table S3. The unit cell is very similar to that of compound **2 Ce** and is closely isostructural, but the smaller ionic radius of Dy^{3+} results in a change of the

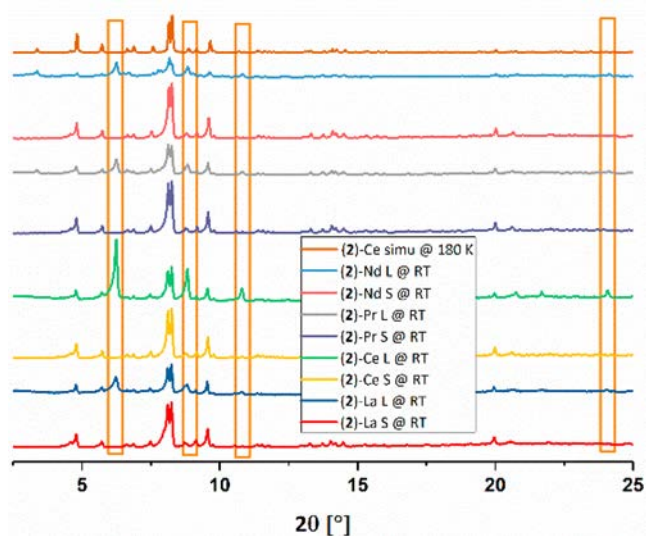


Figure 7. PXRD patterns of the 2 Ln family (with Ln = La–Nd). Abbreviations: simu, simulation; S, stirring method; L, layering method. The 2θ values of reflections of the byproducts are highlighted in orange boxes.

monoclinic space group from $P2_1$ to the centrosymmetric space group $P2_1/c$. The framework structure of compound 3 Dy is shown in Figure 8 and consists of three $\{(\text{MnMo}_6\text{O}_{18})((\text{OCH}_2)_3\text{CNHCH}_2(\text{C}_6\text{H}_4)\text{COO})_2\}^{5-}$ moieties, two $\{\text{Dy}(\text{DMF})_4(\text{H}_2\text{O})\}^{3+}$ moieties, and one $\{\text{Dy}_3(\text{DMF})_6\}^{9+}$ moiety. Furthermore, five DMF molecules can be identified in the lattice by using the OLEX2 solvent mask.⁴⁰

For a simple description of the structure, A E POMs with different coordination modes are marked in different colors. As shown in Figure 8b, the red A E POM coordinates to two $\{\text{Dy}(\text{DMF})_4(\text{H}_2\text{O})\}^{3+}$ units (Dy1) via two terminal oxygen atoms. Additionally, these Dy^{3+} ions are further linked to the green hybrids by one terminal oxygen atom, resulting in a coordination number of 8. Within this part of the structure (Figure 9) the Dy–Mn distances are 6.1 and 6.8 Å and the Mn–Mn distance between one green and one red hybrid is 12.1 Å. The Mn–Mn distance between two green POMs amounts to 23.6 Å. The Dy–Dy distance is 12.1 Å. The

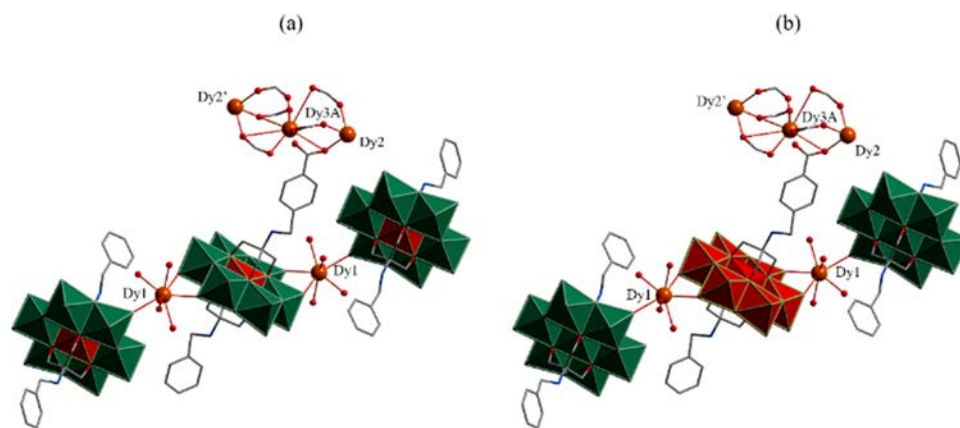


Figure 8. Structure of compound 3 Dy. Color code: A E POMs, green ring with red polyhedral models (a); A E POMs, green and red polyhedral models (b); Dy, orange; O, red; C, gray wire/stick; N, blue wire/stick. Lattice DMF molecules and H atoms are omitted for clarity. DMF and H_2O molecules of the $\{\text{Dy}(\text{DMF})_4(\text{H}_2\text{O})\}^{3+}$ units are represented by their O atoms. DMF molecules of the $\{\text{Dy}_3(\text{DMF})_6\}^{9+}$ moiety are omitted for clarity.

distance of one O_{COO} functional group to the other within one hybrid ranges from 22.7 to 22.9 Å, which in comparison to the free hybrid 1 is compressed on average by 0.3 Å.

As a result of the presence of an inversion center and a c glide in the space group $P2_1/c$ only one mono Dy unit is represented rather than the two Ce units (unit 1 and unit 2) for the compound 2 Ce.

The SHAPE³⁹ analysis shows that the Dy1 ion is square antiprismatic (SAPR) 8 fold coordinated (Table S5 and Figure S24).

In addition, the carboxylate groups of the hybrids coordinate to the $\{\text{Dy}_3(\text{DMF})_6\}^{9+}$ moiety, where the ratio of red to green polyanions coordinating to this core is 2:4 (Figure 10b). In comparison to the environment of the 2 family (Figure 10a), two blue POMs become equivalent to the green POMs. The inversion center of the centrosymmetric space group $P2_1/c$ in the crystal structure of 3 Dy is between Dy3 and its inversion equivalent Dy3A within the $\{\text{Dy}_3(\text{DMF})_6\}^{9+}$ moiety. Due to this inversion center the middle Dy atom of the $\{\text{Dy}_3(\text{DMF})_6\}^{9+}$ unit is disordered. Furthermore, the coordinating carboxylate groups and the phenyl groups bound to these carboxylate groups are also disordered (kink at N disorder). Nevertheless, the 2 fold disorder could be modeled for all of the organic ligands.

Due to the high degree of disorder, it was not possible to determine the geometries of the Dy atoms within the $\{\text{Dy}_3(\text{DMF})_6\}^{9+}$ unit. When a dummy atom was placed between the 2 fold disordered Dy3 atom (Dy3A and Dy3B) (Figure S25) approximate distances of 12.6–13.5 Å between the Dy atoms of the $\{\text{Dy}_3(\text{DMF})_6\}^{9+}$ moiety to the Mn atoms of the L–POM–L units could be estimated.

Figure 11 shows the PXRD patterns of the series 3 Ln with Ln = Y, Sm–Lu. The simulated pattern (3 Dy simu) serves as a reference. It is clearly seen that all of the measured samples, including those with L (synthesized via layering method) and S (synthesized under stirring conditions), correlate with 3 Dy simu. However, the synthesis under stirring conditions was only successful in the case of Dy; in all other cases the PXRD patterns did not agree with the simulated pattern. For this reason, these patterns are not shown in Figure 11.

Topological Analyses. Families 2 and 3 both form complex 3D structures, and therefore their topological analyses

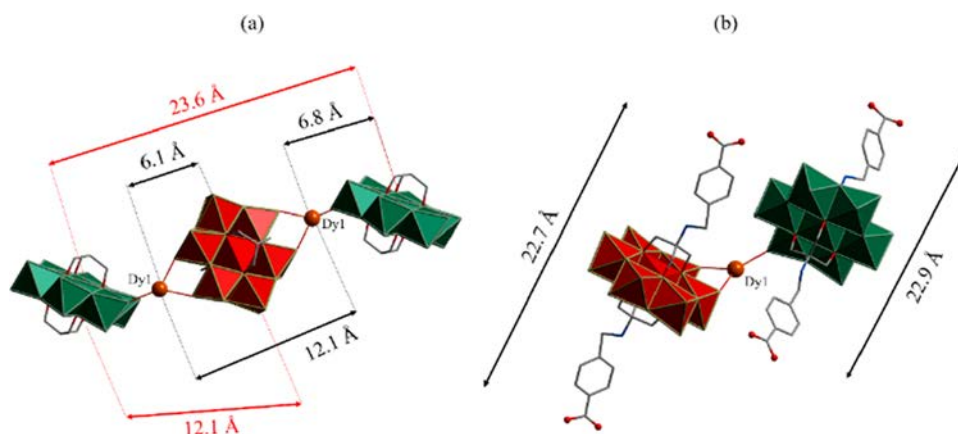


Figure 9. Extracts of the structure of 3 Dy. Color code: A E POMs, green and red polyhedral models; Dy, orange; O, red; C, gray wire/stick; N, blue wire/stick. DMF, water molecules, and H atoms are omitted for clarity.

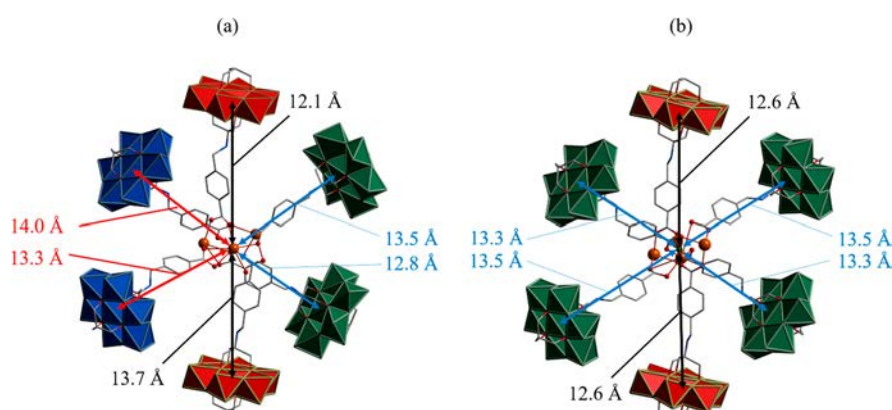


Figure 10. Comparison of the Ln₃ environment of the 2 (a) and 3 (b) families. Color code: A E POMs: green, red, and blue polyhedral models; Ln, orange; O, red; C: gray wire/stick; N, blue wire/stick. DMF, water molecules, and H atoms are omitted for clarity.

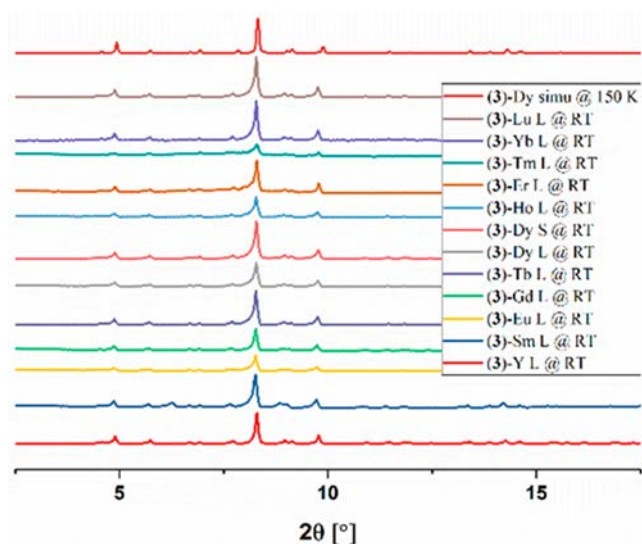


Figure 11. PXRD patterns of the 3 Ln series (with Ln = Y, Sm–Lu). Abbreviations: simu, simulation; S, stirring method; L, layering method.

are helpful. As shown on the left side of Figure 12, a topological analysis reveals that the structure of compound 2 Ce includes four topologically different units. The structure contains two Mn^{III} cores resulting from two independent

{(MnMo₆O₁₈)((OCH₂)₃CNHCH₂(C₆H₄)COO)₂} units (green and blue spheres), providing triply coordinating linker hybrids (Figure 12i,ii). Furthermore, there is one MnCe₂ unit, which is based on one {(MnMo₆O₁₈)((OCH₂)₃CNHCH₂(C₆H₄)COO)₂}, one {Ce³⁺(DMF)₆} (Ce1), and one {Ce³⁺(DMF)₅} (Ce2) unit (red spheres, Figure 12iii). The hybrid coordinates to the Ce cations via two terminal atoms of two diametrically opposed POM moieties. Thus, this crystallographically potentially 6 fold linker now extends to the Ce cations and becomes a 4 fold linker from a topological point of view. Topologically (Figure 12a) blue and green spheres are linked to the red spheres, which corresponds to the coordination of the blue and green labeled A E POM moieties of the hybrids to the Ce1 and Ce2 ions, respectively, via the terminal oxygen atoms of the POMs shown in Figure 6. The fourth component of the topology is provided by the Ce₃ centers originating from one {Ce₃⁹⁺(DMF)₁₀} unit (purple sphere, Figure 12iv). As shown in Figure 12, it is clearly seen that each purple sphere is hexagonally connected to two green, two blue, and two red spheres. This corresponds to the coordination of the POM hybrids to the {Ce₃⁹⁺(DMF)₁₀} moiety via the carboxylate groups. The topology of this structure can be discussed in two ways. (i) The A E POM hybrids are 3 and 6 fold linkers, respectively, connected to each other via the coordination of terminal oxygen atoms to Ce ions (Ce1 and Ce2), and the {Ce₃⁹⁺(DMF)₁₀} units represent the nodes, which are hexagonally coordinated by the

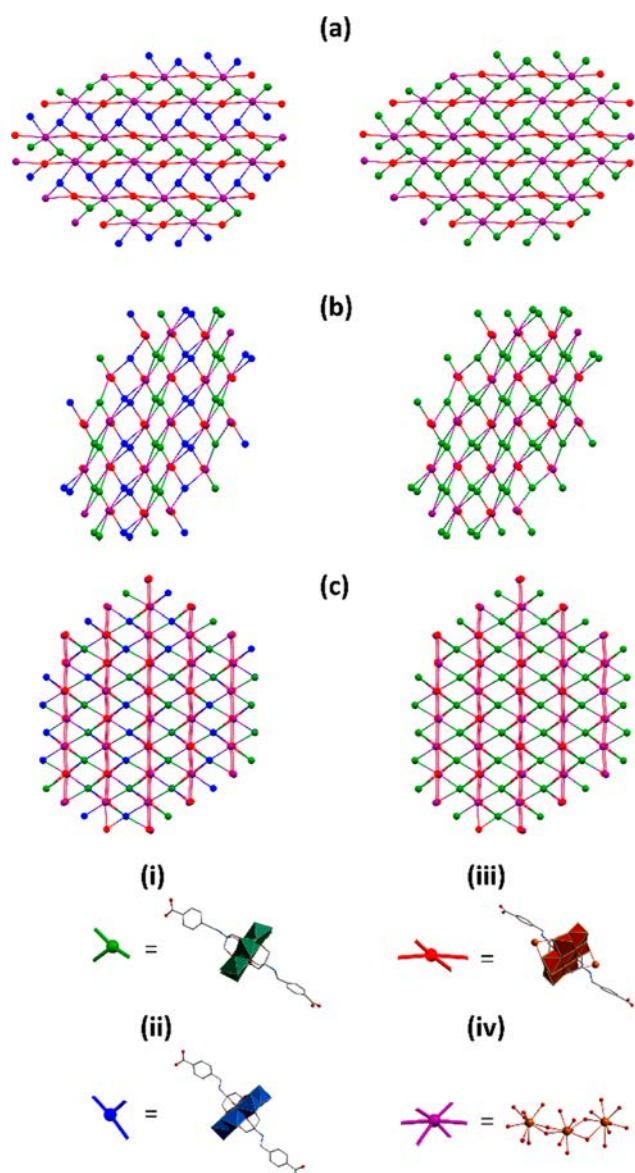


Figure 12. Comparison of the topology of the 2 family (left side) to the 3 family (right side): topological nets along the *a* axis (a), *b* axis (b) and *c* axis (c) created from the L–POM–L 3 connecting unit, shown in green and blue, the 4 connecting unit shown in red, and 6 connecting unit, which is the Ln₃ unit.

carboxylate groups of the POM linkers. (ii) Every colored sphere in the topological representation of this structure is a node, which means that all of the POM moieties of the POM hybrids become a junction. As a result, if the structure is viewed in this way, the organic residues and the Ce1 and Ce2 ions now become the connecting units.

The topology can be identified as a 3,4,6 coordinated 3 nodal net with ToposPro point symbol $\{6^{10}.8^3.10^2\}\{6^3\}2\{6^5.10\}$ and labeled as 3,4,6T281.⁴¹

A topological analysis of 3 Dy reveals that the structure has the same topology as that of the closely isostructural compound 2 Ce. In Figure 12 the topology of the 2 family (left side) is compared to the 3 family (right side). Due to the change in space group from acentric $P2_1$ (2 family) to the centrosymmetric space group $P2_1/c$ (3 family), the blue spheres in the topology of the 2 family become equivalent to the green spheres in the topology of the 3 family.

Given that both families of structures exhibit the same topology, it is pertinent to check that the acentric space group for the 2 family is correct and that an inversion symmetry has not been missed. The crystal structure of 2 Ce refines in the space group $P2_1$ with a Flack χ parameter of 0.125(4) for a Friedel coverage of 82.4%. This indicates that the crystal used for the measurement was partially twinned by inversion, such that 87.5% of the crystal was made up of domains in which the structure has the same handedness as the refined structure, with 12.5% consisting of domains of the opposite enantiomer. The magnitude of the standard uncertainty in the refined Flack parameter (0.004) is in good agreement with the expected value estimated from the amount of resonant scattering in the structure (0.003). In contrast, for a genuinely centrosymmetric structure refined (incorrectly) in $P2_1$, one would expect χ to take a value close to 0.5, with a standard uncertainty much higher than that found here.⁴² Conversely, attempts to refine the structure of 3 Dy in $P2_1$ rather than $P2_1/c$ led to severe correlation between parameters that are related by the $P2_1/c$ inversion symmetry, and the disorder of the Dy₃ moiety still could not be resolved.

It is clear that in the 3 family, in which the heavier but smaller lanthanide cations have a lower coordination number and fewer DMF ligands on the trinuclear Ln₃ moiety, any ordering of the orientation of that moiety must be at best short range in nature. For the 2 family, on the other hand, the larger ionic radii of Ln³⁺ has resulted in a Ln₃ unit with 10 rather than 6 DMF ligands, and this unit now shows long range ordering, with the resulting ordered domains being large enough to diffract in their own right, even if this ordering did not extend through the complete crystal.

We note that, within a batch of a compound from the 2 family, one enantiomer of the structure will dominate in some crystals and the opposite enantiomer in others. Furthermore, the numbers of such crystals will be equal, such that a polycrystalline batch forms a racemic conglomerate.⁴³ As Flack points out, a consequence of this is that a technique such as CD spectroscopy will not be able to detect the chirality of the structure from a polycrystalline sample.

CONCLUSIONS

We have developed an elegant triad approach involving flexible building units of a POM, an organic ligand, and lanthanides to develop a third route for constructing POMOFs. We not only have used a new approach to combining POMs using MOF design principles but have also performed topological analyses and identified an interesting switch from an achiral to a chiral space group without changing the underlying topology. These findings are of interest in terms of the potential of chiral switching in framework materials. The properties of these newly explored POMOFs are under investigation.

AUTHOR INFORMATION

Corresponding Authors

Marcel P. Merkel – Institute of Nanotechnology, Karlsruhe Institute of Technology Campus North, 76344 Eggenstein Leopoldshafen Karlsruhe, Germany; Institute of Inorganic Chemistry, Karlsruhe Institute of Technology, 76131 Karlsruhe, Germany;
Email: marcel.merkel@kit.edu

Annie K. Powell – Institute of Nanotechnology, Karlsruhe Institute of Technology Campus North, 76344 Eggenstein Leopoldshafen Karlsruhe, Germany; Institute of Inorganic Chemistry, Karlsruhe Institute of Technology, 76131 Karlsruhe, Germany;
Email: annie.powell@kit.edu

Authors

Christopher E. Anson – Institute of Inorganic Chemistry, Karlsruhe Institute of Technology, 76131 Karlsruhe, Germany;

George E. Kostakis – University of Sussex, Brighton BN1 9RH, United Kingdom;

Funding

We thank the Helmholtz POF STN, Helmholtz Association and Karlsruhe House of Young Scientists (KHYS) for funding the short term stay of M.P.M. at the University of Sussex (United Kingdom).

Notes

The authors declare no competing financial interest.

ACKNOWLEDGMENTS

We thank Prof. Dr. Dieter Fenske and Dr. Olaf Fuhr for collecting the crystallographic data.

REFERENCES

- (1) According to IUPAC this is the relationship between CPs and MOFs: a metal–organic framework, abbreviated MOF, is a coordination polymer (or alternatively coordination network) with an open framework containing potential voids: Batten, S. R.; Champness, N. R.; Chen, X. M.; Garcia Martinez, J.; Kitagawa, S.; Öhrström, L.; O’Keeffe, M.; Suh, M. P.; Reedijk, J. Coordination polymers, metal organic frameworks and the need for terminology guidelines. *CrystEngComm* **2012**, *14*, 3001–3004.
- (2) Brown, K.; Zolezzi, S.; Aguirre, P.; Venegas Yazigi, D.; Paredes Garcia, V.; Baggio, R.; Novak, M. A.; Spodine, E. [Cu(H₂btec)(bipy)]_∞: a novel metal organic framework (MOF) as heterogeneous catalyst for the oxidation of olefins. *Dalton Trans.* **2009**, 1422–1427.
- (3) Rowsell, J. L. C.; Eckert, J.; Yaghi, O. M. Characterization of H₂ Binding Sites in Prototypical Metal Organic Frameworks by Inelastic Neutron Scattering. *J. Am. Chem. Soc.* **2005**, *127*, 14904–14910.
- (4) Siegelman, R. L.; McDonald, T. M.; Gonzalez, M. I.; Martell, J. D.; Milner, P. J.; Mason, J. A.; Berger, A. H.; Bhowan, A. S.; Long, J. R. Controlling Cooperative CO₂ Adsorption in Diamine Appended Mg₂(dobpdc) Metal–Organic Frameworks. *J. Am. Chem. Soc.* **2017**, *139*, 10526–10538.
- (5) Lennartson, A.; McKenzie, C. J. Bridging nitrile groups in a metal organic framework. *J. Coord. Chem.* **2012**, *65*, 4194–4202.

- (6) Bendi, R.; Kumar, V.; Bhavanasi, V.; Parida, K.; Lee, P. S. Metal Organic Framework Derived Metal Phosphates as Electrode Materials for Supercapacitors. *Adv. Energy Mater.* **2016**, *6*, 1501833.

- (7) Liu, J.; Lukose, B.; Shekhah, O.; Arslan, H. K.; Weidler, P.; Gliemann, H.; Bräse, S.; Grosjean, S.; Godt, A.; Feng, X.; Müllen, K.; Magdau, I. B.; Heine, T.; Wöll, C. A novel series of isorecticular metal organic frameworks: realizing metastable structures by liquid phase epitaxy. *Sci. Rep.* **2012**, *2*, 1–5.

- (8) Song, G.; Wang, Z.; Wang, L.; Li, G.; Huang, M.; Yin, F. Preparation of MOF(Fe) and its catalytic activity for oxygen reduction reaction in an alkaline electrolyte. *Chin. J. Catal.* **2014**, *35*, 185–195.

- (9) Bauer, S.; Stock, N. Funktionale poröse Materialien: MOFs Metallorganische Gerüststrukturen. *Chem. Unserer Zeit* **2008**, *42*, 12–19.

- (10) Huheey, J.; Keiter, E.; Keiter, R. *Anorganische Chemie Prinzipien von Struktur und Reaktivität*, 5th ed.; De Gruyter: Berlin, 2014.

- (11) Nohra, B.; El Moll, H.; Rodriguez Albelo, L. M.; Mialane, P.; Marrot, J.; Mellot Draznieks, C.; O’Keeffe, M.; Ngo Biboum, R.; Lemaire, J.; Keita, B.; Nadjro, L.; Dolbecq, A. Polyoxometalate Based Metal Organic Frameworks (POMOFs): Structural Trends, Energetics, and High Electrocatalytic Efficiency for Hydrogen Evolution Reaction. *J. Am. Chem. Soc.* **2011**, *133*, 13363–13374.

- (12) Hagrman, D.; Zubieta, C.; Rose, D. J.; Zubieta, J.; Haushalter, R. Composite aus eindimensionalen Koordinationspolymeren Matrizes und Molybdanoxid Untereinheiten: Polyoxomolybdatcluster in [Cu(4,4’ bpy)]₄Mo₈O₂₆] und [Ni(H₂O)₂(4,4’ bpy)₂]₂Mo₈O₂₆] und eindimensionale Oxidketten in [Cu(4,4’ bpy)]₄Mo₁₅O₄₇·8H₂O. *Angew. Chem.* **1997**, *109*, 904–907.

- (13) Rafiee, E.; Nobakht, N. Keggin type heteropoly acid, encapsulated in metal organic framework: A heterogeneous and recyclable nanocatalyst for selective oxidation of sulfides and deep desulfurization of model fuels. *J. Mol. Catal. A: Chem.* **2015**, *398*, 17–25.

- (14) Zhang, Z. M.; Zhang, T.; Wang, C.; Lin, Z.; Long, L. S.; Lin, W. Photosensitizing Metal–Organic Framework Enabling Visible Light Driven Proton Reduction by a Wells–Dawson Type Polyoxometalate. *J. Am. Chem. Soc.* **2015**, *137* (9), 3197–3200.

- (15) Du, D. Y.; Qin, J. S.; Li, S. L.; Su, Z. M.; Lan, Y. Q. Recent advances in porous polyoxometalate based metal–organic framework materials. *Chem. Soc. Rev.* **2014**, *43*, 4615–4632.

- (16) Wang, X.; Chang, Z.; Lin, H.; Tian, A.; Liu, G.; Zhang, J. Assembly and photocatalysis of two novel 3D Anderson type polyoxometalate based metal–organic frameworks constructed from isomeric bis(pyridylformyl)piperazine ligands. *Dalton Trans.* **2014**, *43*, 12272–12278.

- (17) Song, J.; Luo, Z.; Britt, D. K.; Furukawa, H.; Yaghi, O. M.; Hardcastle, K. I.; Hill, C. L. A Multiunit Catalyst with Synergistic Stability and Reactivity: A Polyoxometalate Metal Organic Framework for Aerobic Decontamination. *J. Am. Chem. Soc.* **2011**, *133*, 16839–16846.

- (18) Li, X. X.; Wang, Y. X.; Wang, R. H.; Cui, C. Y.; Tian, C. B.; Yang, G. Y. Designed Assembly of Heterometallic Cluster Organic Frameworks Based on Anderson Type Polyoxometalate Clusters. *Angew. Chem., Int. Ed.* **2016**, *55*, 6462–6466.

- (19) Wei, M.; Wang, X.; Duan, X. Crystal Structures and Proton Conductivities of a MOF and Two POM–MOF Composites Based on Cu^{II} Ions and 2,2’ Bipyridyl 3,3’ dicarboxylic Acid. *Chem. Eur. J.* **2013**, *19*, 1607–1616.

- (20) Wei, M.; Wang, X.; Sun, J.; Duan, X. A 3D POM–MOF composite based on Ni(II) ion and 2,2’ bipyridyl 3,3’ dicarboxylic acid: Crystal structure and proton conductivity. *J. Solid State Chem.* **2013**, *202*, 200–206.

- (21) Yang, H.; Li, J.; Zhang, H.; Lv, Y.; Gao, S. Facile synthesis of POM@MOF embedded in SBA 15 as a steady catalyst for the hydroxylation of benzene. *Microporous Mesoporous Mater.* **2014**, *195*, 87–91.

- (22) Sha, J.; Huang, L.; Peng, J.; Pang, H.; Tian, A.; Zhang, P.; Chen, Y.; Zhu, M. Assembly of two novel Lindqvist polyoxoanion templated

coordination polymers with standard honeycomb cavities. *Solid State Sci.* **2009**, *11*, 417–421.

(23) Shi Zhou; Kong, Z. G.; Wang, Q. W.; Li, C. B. A novel polyoxometalate templated chiral three fold interpenetrated metal organic framework: Synthesis, structure and properties. *Inorg. Chem. Commun.* **2012**, *20*, 131–134.

(24) Marleny Rodriguez Albelo, L.; Ruiz Salvador, A. R.; Sampieri, A.; Lewis, D. W.; Gomez, A.; Nohra, B.; Mialane, P.; Marrot, J.; Secheresse, F.; Mellot Draznieks, C.; Ngo Biboum, R.; Keita, B.; Nadjo, L.; Dolbecq, A. Zeolitic Polyoxometalate Based Metal Organic Frameworks (Z POMOFs): Computational Evaluation of Hypothetical Polymorphs and the Successful Targeted Synthesis of the Redox Active Z POMOF1. *J. Am. Chem. Soc.* **2009**, *131*, 16078–16087.

(25) Qin, J. S.; Du, D. Y.; Guan, W.; Bo, X. J.; Li, Y. F.; Guo, L. P.; Su, Z. M.; Wang, Y. Y.; Lan, Y. Q.; Zhou, H. C. Ultrastable Polymolybdate Based Metal–Organic Frameworks as Highly Active Electrocatalysts for Hydrogen Generation from Water. *J. Am. Chem. Soc.* **2015**, *137*, 7169–7177.

(26) Li, S.; Ma, H.; Pang, H.; Zhang, L.; Zhang, Z.; Lin, H. The first 3D POMOF based on α metatungstate and mixed ligand. *Inorg. Chem. Commun.* **2014**, *44*, 15–19.

(27) Zhu, P. P.; Sun, L. J.; Sheng, N.; Sha, J. Q.; Liu, G. D.; Yu, L.; Qiu, H. B.; Li, S. X. Tuning the Helical Structures of Wells–Dawson Polyoxometalate Based Hybrid Compounds by Using Isomeric Ligands. *Cryst. Growth Des.* **2016**, *16*, 3215–3223.

(28) Yazigi, F. J.; Wilson, C.; Long, D. L.; Forgan, R. S. Synthetic Considerations in the Self Assembly of Coordination Polymers of Pyridine Functionalized Hybrid Mn Anderson Polyoxometalates. *Cryst. Growth Des.* **2017**, *17*, 4739–4748.

(29) Han, J. W.; Hill, C. L. A Coordination Network That Catalyzes O₂ Based Oxidations. *J. Am. Chem. Soc.* **2007**, *129*, 15094–15095.

(30) Blazevic, A.; Rompel, A. The Anderson–Evans polyoxometalate: From inorganic building blocks via hybrid organic–inorganic structures to tomorrows “Bio POM. *Coord. Chem. Rev.* **2016**, *307*, 42–64.

(31) Pope, M. T. Heteropoly and Isopoly Oxometalates. In *Inorganic Chemistry Concepts*; Springer Verlag: Berlin, 1983; Vol. 8.

(32) Yin, P.; Bayaguud, A.; Cheng, P.; Haso, F.; Hu, L.; Wang, J.; Vezenov, D.; Winans, R. E.; Hao, J.; Li, T.; Wei, Y.; Liu, T. Spontaneous Stepwise Self Assembly of a Polyoxometalate–Organic Hybrid into Catalytically Active One Dimensional Anisotropic Structures. *Chem. Eur. J.* **2014**, *20*, 9589–9595.

(33) Zhao, C.; Ma, H.; Pang, H.; Li, S.; Zhang, Z.; Yu, Y. A new POMOF consisting of [VW₁₂]⁴⁺ clusters and metal organic nano tubes: Synthesis, structure, electrocatalytic and luminescent properties. *Inorg. Chem. Commun.* **2016**, *69*, 57–61.

(34) Chai, D. F.; Wang, M.; Zhang, C.; Ning, F.; Xu, W.; Pang, H.; Ma, H. A novel 3D POMOF based on dinuclear copper (II) oxalate complexes and Keggin polyoxoanions with excellent photocatalytic activity. *Inorg. Chem. Commun.* **2017**, *83*, 16–19.

(35) Li, L.; Sun, J. W.; Sha, J. Q.; Li, G. M.; Yan, P. F.; Wang, C. Construction of POMOFs with different degrees of interpenetration and the same topology. *CrystEngComm* **2015**, *17*, 633–641.

(36) Ginsberg, A. P. *Inorganic Syntheses*; Wiley: 1990; p 27.

(37) Hill, C. L.; Anderson, T. M.; Han, J. W.; Hillesheim, D. A.; Geletii, Y. V.; Okun, N. M.; Cao, R.; Botar, B.; Musaev, D. G.; Morokuma, K. New complexes and materials for O₂ based oxidations. *J. Mol. Catal. A: Chem.* **2006**, *251*, 234–238.

(38) Spek, A. L. PLATON SQUEEZE: a tool for the calculation of the disordered solvent contribution to the calculated structure factors. *Acta Crystallogr., Sect. C: Struct. Chem.* **2015**, *71*, 9–18.

(39) Llunell, M.; Casanova, D.; Cirera, J.; Alvarez, S.; Alemany, P. *SHAPE: Program for the Stereochemical Analysis of Molecular Fragments by Means of Continuous Shape Measures and Associated Tools, ver. 2.1*; Universitat de Barcelona: Barcelona, 2013.

(40) Dolomanov, O. V.; Bourhis, L. J.; Gildea, R. J.; Howard, J. A. K.; Puschmann, H. OLEX2: a complete structure solution, refinement and analysis program. *J. Appl. Crystallogr.* **2009**, *42*, 339–341.

(41) Blatov, V. A.; Shevchenko, A. P.; Proserpio, D. M. Applied Topological Analysis of Crystal Structures with the Program Package ToposPro. *Cryst. Growth Des.* **2014**, *14*, 3576–3586.

(42) Flack, H. D.; Bernardinelli, G.; Clemente, D. A.; Linden, A.; Spek, A. L. Centrosymmetric and Pseudo Symmetric Structures Refined as Non Centrosymmetric. *Acta Crystallogr., Sect. B: Struct. Sci.* **2006**, *B62*, 695–701.

(43) Flack, H. D. Chiral and Achiral Crystal Structures. *Helv. Chim. Acta* **2003**, *86*, 905–921.

Repository KITopen

Dies ist ein Postprint/begutachtetes Manuskript.

Empfohlene Zitierung:

Merkel, M. P.; Anson, C. E.; Kostakis, G. E.; Powell, A. K.

[Taking the Third Route for Construction of POMOFs: The First Use of Carboxylate-Functionalized MnIIIAnderson-Evans POM-Hybrid Linkers and Lanthanide Nodes.](#)

2021. Crystal Growth and Design, 21.

doi: [10.5445/IR/1000133858](#)

Zitierung der Originalveröffentlichung:

Merkel, M. P.; Anson, C. E.; Kostakis, G. E.; Powell, A. K.

[Taking the Third Route for Construction of POMOFs: The First Use of Carboxylate-Functionalized MnIIIAnderson-Evans POM-Hybrid Linkers and Lanthanide Nodes.](#)

2021. Crystal Growth and Design, 21 (6), 3179–3190.

[doi:10.1021/acs.cgd.0c01138](#)

Lizenzinformationen: [KITopen-Lizenz](#)